Latin American Journal of Solids and Structures
www.lajss.org

Transient heat conduction in multiwall carbon nanotubes

Abstract

In this paper, theoretical investigation is performed on two-dimensional transient heat conduction in multiwall carbon nanotubes (MWCNTs) by using a continuum model. Temperature, size and direction dependencies of thermal properties are considered. Both Fourier and non-Fourier heat conduction approaches are used and finite element models are developed to solve the nonlinear equations for MWCNTs. The presented solutions are verified by comparing the results with those reported in the literature. Three types of thick and thin MWCNTs are considered and thermal shock is applied to their cylindrical surfaces or end cross sectional areas. Temperature distributions resulted from both approaches are obtained and compared together. Interesting results are found especially in MWCNTs that are exposed to extreme temperature gradient.

Keywords

Non-Fourier heat conduction; multiwall carbon nanotube; finite element method; thermal shock.

M. Tahani [a]
M.H. Abolbashari [b]
S.T. Talebian [c*]
B. Mehrafrooz [d]
H. Saberi Nik [c]

[a] Department of Mechanical Eng., Faculty of Eng., Ferdowsi University of Mashhad, Mashhad, Iran,
e-mail: mtahani@um.ac.ir
[b] Dep. of Mech. Eng., Lean Production Eng. Res. Center, Ferdowsi Univ. of Mashhad, Mashhad, Iran, e-mail: abolbash@um.ac.ir
[c] Young Res. and Elite Club, Neyshabur Branch, Islamic Azad Univ., Neyshabur, Iran,
e-mail: saberi_hssn@yahoo.com
[d] Dep. Mech. Eng., Sharif Univ. Technology, Tehran, Iran, e-mail:
mehrafrooz_behzad@sharif.edu

Corresponding author:
*taha_talebian@yahoo.com

http://dx.doi.org/10.1590/1679-78251374

Received 24.05.2014
In revised form 18.09.2014
Accepted 21.10.2014
Available online 11.11.2014

1 INTRODUCTION

The past decade was full of countless achievements in nano engineering area. One of those advancements is carbon nanotubes (CNTs) (Usmani and Hassan, 2010; Bokobza, 2007; Cassell and Li, 2007; Dasgupta et al., 2011; Du et al., 2008; Endo et al., 2008; Fam et al., 2011; Fraysse et al., 2002). An individual CNT either consists of single tube and called single wall carbon nanotube (SWCNT) or of several tubes called MWCNT. CNTs have attracted great interest from research community due to not only their electronic and mechanical properties but also for their unique

thermal properties. CNTs have many potential applications such as thermal management of microsystems, so investigating thermal behavior of CNTs is important.

In similarity to Ohm's rule for electrical conductors, Fourier's law is an empirical law of heat transfer in solids which utters that the thermal conductance of a material scales inversely with its length or, equivalently, that the thermal conductivity is independent of sample length. While Fourier's law is well founded for virtually all thermal conductors that have been experimentally probed, attempts towards supplying a rigorous theoretical basis for it have broke down. Theoretical examines have established that Fourier's law is broke for a variety of one-dimensional systems. CNTs are one-dimensional materials, Thus, they are suited for experimental investigations of the validity of Fourier's law in a low dimension (Chang et al., 2008). On the other hand, Fourier's law is only an approximate description of the procedure of conduction, missing the time needed for acceleration of the heat flow. In fact this time required for acceleration of the heat flow is caused by thermal ''inertia", which is realized as the lag consequence of the gradually increased heat flux after the establishment of the temperature gradient like the other ubiquitous generalized fluxes and forces. CNTs have this inertia behavior and so, are not following the Fourier's law (Wang et al., 2010).

Enormous series of studies have carried out to determine the effects of different parameters on mechanical properties of CNTs (Won et al., 2012; Ranjbartoreh et al., 2010; Lu et al., 2010; Li et al., 2009). However, only small part of them has been focused on the influence of thermal conduction on mechanical behavior of CNTs, so it is still challenging to investigate thermal properties of CNTs. Zhang and Li (2005) proposed dependency of the thermal conductivity of SWCNTs on chirality, isotope impurity, tube length, and temperature based on non-equilibrium molecular dynamics method. Moreover, Jeng et al. (2004) studied the thermal effects on tensile and compression deformation of CNTs. Zhu and Wang (2007) demonstrated the effect of temperature on elastic properties of SWCNTs. Talebian et al. (2012a) investigated the effects of temperature on the axisymmetric dynamic behavior of MWCNTs. Later, they (Talebian et al., 2012b) analytically studied dynamic behavior of MWCNTs under thermal shock synchronized on all tubes. But, if thermal shock is applied to a particular boundary of a MWCNT, temperature distributions are deferent at any layer and it is not homogeneous so it is necessary to find temperature distributions by heat conduction analysis.

On the other hand, a heat conduction analysis of MWCNTs is not regular because the mechanism of heat conduction in CNTs is complex; Since, non-Fourier heat conduction effects in CNTs, cannot be disregarded (Chang et al., 2008). In non-Fourier heat conduction theory, a delay time exists between temperature gradient and heat flow. Therefore, even there is not temperature gradient between two points, heat transfer remains and heat fluxes move for a small time. This delay may be important in micro/nano-scale and cannot be neglected (Wang et al., 2012). Shiomi and Maruyama (2006) investigated non-Fourier heat conduction in CNTs based on classical molecular dynamics simulations. Xu and Li (2012) modeled nano-scale heat conduction with use of the Boltzmann transport equation. Wang et al. (2010) stated that heat conduction in CNTs can be regarded as the motion of the weighty phonon gas governed by its mass and momentum conservation equations. So, it reduces to Fourier heat conduction law as the heat flux is not very high and the consequent inertial force of phonon gas is negligible. Also, Wang et al. (2011) investigat-

ed non-Fourier heat conduction in nanomaterials by use of the thermomass theory. Hu and Cao (2012) investigated heat conduction in CNTs based on non-equilibrium molecular dynamics simulations. By the same method, Zhang et al. (2012) studied thermal transport in a SWCNT bridging two Silicon slabs under constant high heat flux.

In several works, rate of heat conduction in CNTs was first obtained by experimental or molecular dynamics methods (Hu and Cao, 2012; Aliev et al., 2010; Wang and Guo, 2010; Lindsy et al., 2010). Then, the effective thermal conductivity coefficients were estimated by employing equivalent continuum structures (Thomas et al., 2010; Gonzales et al., 2004; Yang et al., 2002). These effective coefficients are useful for estimating general rate of heat conduction in many thermal applications. But, they are inaccurate for transient analysis of MWCNTs because there exists inaccuracy in estimating transient temperature distributions in MWCNTs by using Fourier heat conduction analysis with effective coefficients. In this paper, transient distributions of temperature in MWCNTs under various thermal shocks are obtained with Fourier and non-Fourier methods and compared with available results for assessing this inaccuracy. For this purpose, temperature, size and direction dependencies of thermal properties are considered and finite element models are developed to solve the nonlinear equations. Also, many remarkable results are found for thick and thin MWCNTs under different types of thermal shocks.

2 HEAT CONDUCTION ANALYSIS IN MWCNTS

Here, the Fourier and non-Fourier heat conduction laws are used to investigate transient heat conduction in MWCNTs. A MWCNT is simulated with a continuum model based on multiple elastic shells. Due to intense dependency of CNT's properties on temperature and geometric parameters, the finite element method is used for analyzing heat conduction behavior of MWCNTs under thermal shock. As shown in Fig. 1, the continuum model of a MWCNT is considered with cylindrical coordinate system (r, θ, z) such that the z axis coincides with axis of concentric shells and the origin is at the center of one end of shells.

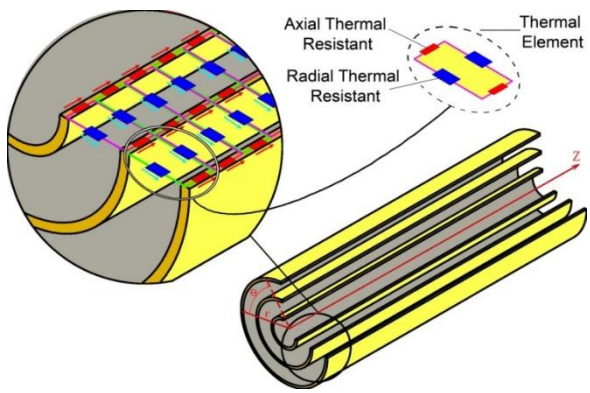

Figure 1: A continuum model for heat conduction analysis of MWCNTs.

2.1 Fourier heat conduction analysis

The two-dimensional transient heat conduction equation in axisymmetric finite length cylinder is (Reddy, 1993):

$$\frac{1}{r}\frac{\partial}{\partial r}\left(k_r r\frac{\partial T}{\partial r}\right)+\frac{\partial}{\partial z}\left(k_z\frac{\partial T}{\partial z}\right)=\rho C_p\frac{\partial T}{\partial t} \tag{1}$$

where T is temperature, k_r and k_z are, respectively, the thermal conductivity coefficients in radial and longitudinal directions, ρ is the mass density and C_p denotes the specific heat capacity. In a MWCNT, there is a strong covalent bond between atoms of arranged lattice in a layer but weak van der Waals connections exist between tubes. Therefore, it is expected that the thermal conductivity coefficient in axial direction to be greater than that of radial direction between tubes. That is, heat conduction in radial and axial directions are different and must be considered precisely in developed model of heat transfer analysis in MWCNTs.

In this study, the finite element method is used to model transient heat conduction in MWCNTs by solving Eq. (1). In this model, rectangular thermal elements are placed between layers which consist of different thermal resistances that connect nodes in longitudinal and radial directions. Multiplying Eq. (1) by weight function w and integrating over cylindrical volume yields:

$$\int w\left(\frac{1}{r}\frac{\partial}{\partial r}\left(k_t r\frac{\partial T}{\partial r}\right)+\frac{\partial}{\partial z}\left(k_z\frac{\partial T}{\partial z}\right)-\rho C_p\dot{T}\right)r\,\mathrm{d}r\,\mathrm{d}z=0 \tag{2}$$

where a dot represents the derivative with respect to time. Then by applying integration by parts for Eq. (2), weak formulation is obtained:

$$\int\left(\frac{\partial w}{\partial r}\left(k_r\frac{\partial T}{\partial r}\right)+\frac{\partial w}{\partial z}\left(k_z\frac{\partial T}{\partial z}\right)+w\rho C_p\dot{T}\right)r\,\mathrm{d}r\,\mathrm{d}z=\oint wq_n\mathrm{d}s \tag{3}$$

where q_n denotes normal heat flux transfer through a given surface which is defined as:

$$q_n=k_r\frac{\partial T}{\partial r}n_r+k_z\frac{\partial T}{\partial r}n_z \tag{4}$$

Temperature is now approximated by summation of linear interpolation function ψ as:

$$T=\sum_{j=1}^{n}\psi_j T_j \tag{5}$$

Also, the weight function is replaced by interpolation functions to obtain:

$$\int\left\{k_r\frac{\partial\psi_i}{\partial r}\frac{\partial\psi_j}{\partial r}T_j+k_z\frac{\partial\psi_i}{\partial z}\frac{\partial\psi_j}{\partial z}T_j+\rho C_p\psi_i\psi_j\dot{T}_j\right\}r\,\mathrm{d}r\,\mathrm{d}z=\oint\psi_i q_n\mathrm{d}s \tag{6}$$

Eq. (6) can be rewritten in matrix form as:

$$\left[C^e\right]\{\dot{T}\} + \left[K^e\right]\{T\} = \{F^e\} \tag{7}$$

where

$$\begin{aligned} C_{ij}^e &= \int \rho C_p \psi_i \psi_j \; r \, \mathrm{d}r \, \mathrm{d}z \\ K_{ij}^e &= \int k_r \frac{\partial \psi_i}{\partial r}\frac{\partial \psi_j}{\partial r} + k_z \frac{\partial \psi_i}{\partial z}\frac{\partial \psi_j}{\partial z} \quad r \, \mathrm{d}r \, \mathrm{d}z \\ F_i^e &= \oint \psi_i q_n \mathrm{d}s \end{aligned} \tag{8}$$

It is noted that the superscript e expresses elemental parameters. Because material properties are related to temperature and geometry parameter, the matrices $[C^e]$, $[K^e]$, and $\{F^e\}$ are calculated for each individual element at each layer of MWCNT and must be updated in every instant of time. Next, through an assemblage process, the global assembled matrices $[K]$, $[M]$ and $\{F\}$ for the whole MWCNT are obtained. Hence, the global form of Eq. (7) can be written as:

$$\left[C\right]\{\dot{T}\} + K\{T\} = \{F\} \tag{9}$$

where $\left[C\right]$ and $\left[K\right]$ are defined as damping and stiffness matrices, respectively, and $\{F\}$ is force vector. Since the material properties are not constant, these matrices are time dependent and change nonlinearly. Therefore, Eq. (9) is a set of nonlinear equations and since the analysis is two-dimensional, the number of its equations is twofold of the number of MWCNT layers and they must be solved simultaneously for each instance of time. Eq. (9) can be solved by utilizing the Newmark technique to obtain transient distribution of temperature.

2.2 Non-Fourier heat conduction analysis

In this section, non-Fourier heat conduction for MWCNTs is developed. In a homogenous body with usual dimensions, steady temperature distribution in one direction is linear. But in an atomic environment with finite particles, temperature distribution is not linear because heat conduction between atoms in such environment does not obey the Fourier law. In this case, by considering the wave theory, longitudinal heat conduction in a CNT is a function of the number of its atoms in longitudinal direction. In carbon nanotubes, atoms arrange regularly so the length of a CNT is related to the number of its particles. Therefore, thermal conductivity coefficient of a CNT in axial direction can be estimated by a function of the length. Several studies verify this idea and up to now, many exponential functions with different coefficients are represented for thermal conductivity coefficient of CNTs (Chang et al., 2008; Zhang and Li, 2005; Ni et al., 2011; Maruyama, 2002; Guo et al., 2009; Volkov and Zhigilei, 2010).

Also, unlike the Fourier heat conduction theory, heat propagates with finite speed in the non-Fourier heat conduction theory. That is, a relaxation time exists between temperature gradient and heat flow which is modeled by the Cattano-Vernotte equation (Moosaie, 2007):

$$\mathbf{q} + \tau_q \frac{\partial \mathbf{q}}{\partial t} = -k\nabla T \tag{10}$$

where $\mathbf{q}$ specifies the heat flow vector and τ_q presents the relaxation time. Substituting Eq. (10) into the energy conservation equation, thermal wave equation takes the form (Wang, 2010):

$$\rho C_p \tau_q \frac{\partial^2 T}{\partial t^2} + \rho C_p \frac{\partial T}{\partial t} = \nabla.(k\nabla T) \tag{11}$$

Initial conditions which represent temperature distribution or heat flow at time zero is considered as $T(r,z,0) = \overline{T}_0(r,z)$ and $\mathbf{q}(r,z,0) = \overline{\mathbf{q}}_0(r,z)$. Eq. (11) for an axisymmetric finite length cylinder can be rewritten as follows:

$$\rho C_p \tau_q \frac{\partial^2 T}{\partial t^2} + \rho C_p \frac{\partial T}{\partial t} = \frac{1}{r}\frac{\partial}{\partial r}\left(k_r r \frac{\partial T}{\partial r}\right) + \frac{\partial}{\partial z}\left(k_z \frac{\partial T}{\partial z}\right) \tag{12}$$

The weak form of Eq. (12) can be obtained as the same procedure presented in the previous section as:

$$\int \left\{ k_r \frac{\partial \psi_i}{\partial r}\frac{\partial \psi_j}{\partial r} T_j + k_z \frac{\partial \psi_i}{\partial z}\frac{\partial \psi_j}{\partial z} T_j + \rho C_p \psi_i \psi_j \dot{T}_j + \rho C_p \tau_q \psi_i \psi_j \ddot{T}_j \right\} r \, \mathrm{d}r \, \mathrm{d}z = \oint \psi_i q_n \mathrm{d}s \tag{13}$$

Eq. (13) can be rewritten in matrix form as:

$$\left[M^e\right]\{\ddot{T}\} + \left[C^e\right]\{\dot{T}\} + \left[K^e\right]\{T\} = \{F^e\} \tag{14}$$

where the matrices $[C^e]$, $[K^e]$, and $[F^e]$ are given by Eq. (8) and $[M^e]$ is defined as:

$$M_{ij}^e = \int \rho C_p \psi_i \psi_j \, r \, \mathrm{d}r \, \mathrm{d}z \tag{15}$$

After assemblage process, the global form of Eq. (14) is:

$$\left[M\right]\{\ddot{T}\} + \left[C\right]\{\dot{T}\} + [K]\{T\} = \{F\} \tag{16}$$

Eq. (16) is a set of nonlinear dynamic equations as Eq. (9) and has the form of a wave equation for a non-regular size and specific shape of a MWCNT. Solution of this equation is more complex than solution of Eq. (9). Wang et al. (2012) developed a numerical technique to solve the non-classical heat conduction equations for the time-dependent temperature field. Here, this technique is generalized for MWCNTs and is applied for solving Eq. (16). Thus, the time the time derivatives are approximated as:

$$\{\dot{T}\}_{n+1} \approx \frac{\{T\}_{n+1} - \{T\}_n}{\Delta t}, \quad \{\ddot{T}\}_{n+1} \approx \frac{\{\dot{T}\}_{n+1} - \{\dot{T}\}_n}{\Delta t} \tag{17}$$

Substitution of Eq. (17) into Eq. (16) results in:

$$\{A\}_{n+1}\{T\}_{n+1} = \{B\}_{n+1} \tag{18}$$

where

$$\begin{aligned} \{A\}_{n+1} &= \frac{[D]}{(\Delta t)^2} + \frac{[C]}{\Delta t} + [K] \\ \{B\}_{n+1} &= \frac{[D]}{\Delta t}\{\dot{T}\}_n + \left(\frac{[D]}{(\Delta t)^2} + \frac{[C]}{\Delta t}\right)\{T\}_n + \{F\}_{n+1} \end{aligned} \tag{19}$$

With identifying $\{T\}_0$ and $\{\dot{T}\}_0$ from initial conditions, $\{T\}_1$ can be obtained from Eq. (18) and then $\{\dot{T}\}_1$ is found from Eq. (17). So, it is straightforward to calculate time history of temperature from Eqs. (17) and (18). Wang et al. (2012) discussed about the accuracy of this numerical solution and concluded that it is unconditionally stable and has the first order of truncation error.

3 RESULTS AND DISCUSSION

As mentioned earlier, properties of CNTs depend on temperature and geometrical parameters. So, there are various values and diagrams for properties of CNTs in literature (Ranjbartoreh et al., 2010; Wang et al., 2009; Pettes and Shi, 2009; Savin et al., 2009; Jiang et al., 2009; Giannopulos et al., 2008). This variety indicates complexity of CNTs behavior and, moreover, diversity of methods and models which are assumed for their performance analyses.

To determine an equivalent continuum structure, tube thickness h and ρh are selected as $h = 0.066$ nm and $\rho h = 7.82 \times 10^{-8}$ g/cm^2, respectively (Talebian et al., 2010). But, the thermal conductivity coefficient is a complicated parameter for CNTs because it is a nonlinear function of temperature, diameter and length of nanotubes. Here, to state the dependency of thermal conductivity coefficient on diameter, ratio of thermal conductivity of CNTs to the thermal conductivity of graphene sheets is used. Variation of this ratio with respect to diameter is considered from studies of Lindsay et al. (2010). Also, variation of the thermal conductivity coefficient of CNTs with respect to length is selected as $k \propto L^{0.32}$ based on the Maruyama model (2002). Moreover, variations of the thermal conductivity coefficient of CNTs via temperature are considered with those obtained by Gu and Chen (2007). Finally, Alive et al. (2010) introduced the ratio of longitudinal thermal conductivity to radial thermal conductivity coefficients between tubes of MWCNTs and estimated it as 342. The same value is assumed in the present study. It is noted that these extracted values of thermal conductivity coefficient are the effective values according to continuum shells model of CNTs. These effective values are generally obtained by applying temperature gradient to two ends of CNT and thermal conductivity coefficients are estimated by calculating heat flow from experimental or computational methods. So, normal equivalent cross section area of CNT affects on thermal conductivity coefficient. In aforesaid investigations, to

calculate equivalent cross sectional area, thickness of each layer is considered to be 0.34 nm which is equal to the distance between tubes and it is deferent with the mentioned value in this paper. Therefore, the extracted values of thermal conductivity coefficient are multiplied by 0.34/0.066 for the present study.

Dependency of chirality and size on the specific heat of CNTs is negligible (Kahaly and Waghmare, 2007). But specific heat in CNTs is a nonlinear function of temperature and should be considered according to the results of Kahaly and Waghmare (2007). The present study is validated by comparing the results of a non-Fourier heat conduction problem with those obtained by Wang et al. (2010). They developed a finite element/finite difference scheme for the non-classical heat conduction and associated thermal stresses. For example, a cylinder with inner and outer radius a and b is considered that is exposed under a thermal shock. Dimensionless parameters are adjusted as follows:

$$\bar{t} = t/\tau_q, \quad \bar{r} = r/l_0, \quad l_0 = \sqrt{K\tau_q/\rho C_p} \tag{20}$$

It is assumed that $\bar{a} = 2$ and $\bar{b} = 5$ and the initial temperature of cylinder is 0° Celsius. Temperature T_0 is applied suddenly to the outer surface while the inner surface is maintained at zero temperature. Radial temperature distributions at $\bar{t} = 1$ and $\bar{t} = 2$ are illustrated in Fig. 2 which are in excellent agreement with the results obtained by Wang et al. (2010).

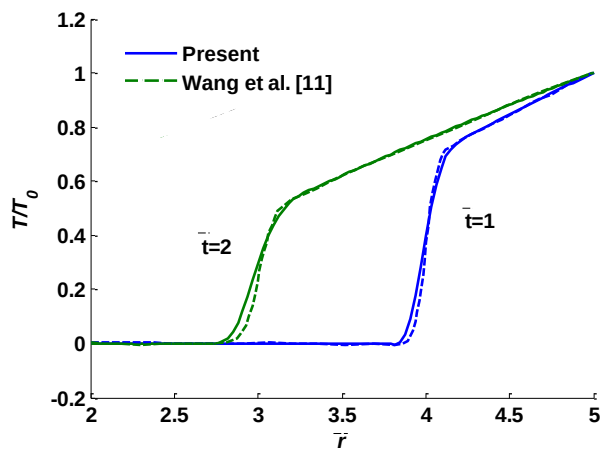

Figure 2: Comparison of radial temperature distributions for a cylinder under external thermal shock.

In the following investigations, three examples of 5- and 13-layer MWCNTs are selected which their geometric data are given in Table 1. The ratio of innermost radius to thickness is named λ and MWCNTs with $\lambda = 1$ and $\lambda = 5$ can be approximately considered as thick and thin, respectively. It is noted that examples 1 and 2 have the same outermost radius and examples 2 and 3 have the same thickness. For all MWCNTs, it is assumed that the ratio of length to outermost radius is equal to 100. Also, boundary thermal conditions are assumed isolated except the surfaces under thermal shock.

3.1 Radial thermal shock

It is necessary to determine the value of relaxation time τ_q. Various values of this parameter for CNTs are reported from 0.025 ps to 226 ps (Nemilentau et al., 2007; Shenogin et al., 2004; Donadio and Gali, 2007). This variety of values can be explained by specific geometry of CNTs which include nano-value in radius and micro-value in length. Small values of τ_q (~1 ps) reveal difference between the Fourier and non-Fourier heat conduction in nano-scale but only larger values of τ_q in range of 100 ps can show this difference in micro-scale. Hence, the values $\tau_q = 1$ ps and $\tau_q = 100$ ps are, respectively, proper for heat conduction analysis in radial and longitudinal directions of CNTs.

	CNT examples		
	1	2	3
Number of layers	13	5	5
Internal radius r_{in}, (nm)	4.08	6.80	1.36
Outermost radius r_{out}, (nm)	8.16	8.16	2.72
Thickness h_m, (nm)	4.08	1.36	1.36
Length (nm)	816	816	272
$\lambda = r_{in} / h_m$	1	5	1

Table 1: Geometric data for three examples of MWCNTs.

Here, it is focused on the distributions of temperature in MWCNTs as illustrated on Figs. 3 and 4. It is assumed that thermal shock with temperature 800 K is applied suddenly to the outermost layer of MWCNTs while the innermost layer remains at initial temperature 300 K. Time histories of transient temperature of layers for middle length point of MWCNTs are illustrated in Fig. 3. In this figure, the results of the Fourier and non-Fourier heat conduction analysis are compared together for three mentioned examples of MWCNTs. Layers of a MWCNT are numbered form the innermost tube to the outermost one and number of each layer is indicated beside each curve. It is seen that with the Fourier heat conduction analysis, temperature of inner tubes increases continuously until it reaches to its equilibrium. But results of the non-Fourier heat conduction analysis for examples 2 and 3 reveals an extremely temperature rise for inner tubes which their temperatures instantly jump to higher temperatures than their equilibrium temperatures. This phenomenon can be simulated mechanically by radial displacements of a MWCNT layers under external pressure shock which displacements increase to values higher than the equilibrium states (Talebian et al., 2013). Therefore, the non-Fourier heat conduction analysis reveals a wave like behavior of heat conduction between layers of a MWCNT.

Heat wave properties depend on geometry parameters of MWCNTs. For example, as illustrated in Fig. 3, rate of temperature variation in 13-layer MWCNT is smaller than 5-layer MWCNTs. Hence, by increasing the number of layers in a MWCNT, intensity of radial heat transfer between its layers decreases. But, the rates of temperature variation in examples 2 and 3 of MWCNTs are approximately the same. So, tubes diameter has not a significant effect on the heat transfer between layers of a MWCNT under external thermal shock.

Here, it is assumed that the temperature 800 K is applied suddenly to the both innermost and outermost layers of MWCNTs. Time histories of transient temperatures for middle length point of three mentioned examples of MWCNTs are illustrated in Fig. 4 which the results of the Fourier and non-Fourier heat conduction analysis are compared together. Layers are numbered from the innermost tube to outermost one which is shown near the curve of each tube. It is seen that with the Fourier heat conduction analysis, the rate of temperature increase is high initially and decreases gradually. So, temperature of each layer increases continuously until it reaches to its equilibrium state. Since the temperatures of innermost and outermost tube remain at 800 K, temperature of all layers finally reaches to this temperature.

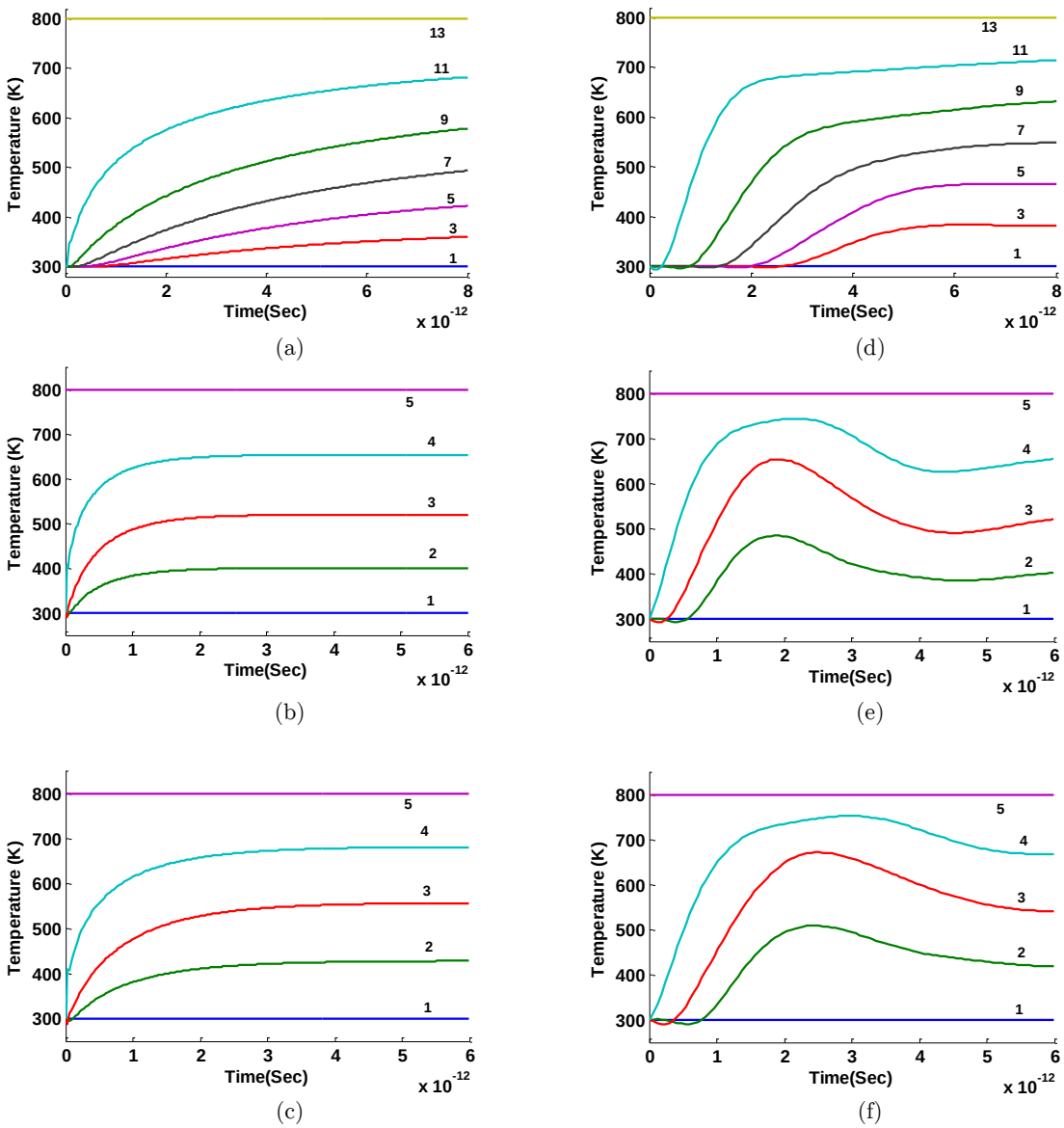

Figure 3: Fourier temperature distributions of examples (a) 1, (b) 2 and (c) 3 of MWCNTs under external thermal shock. (d), (e) and (f) are, respectively, corresponding non-Fourier distributions.

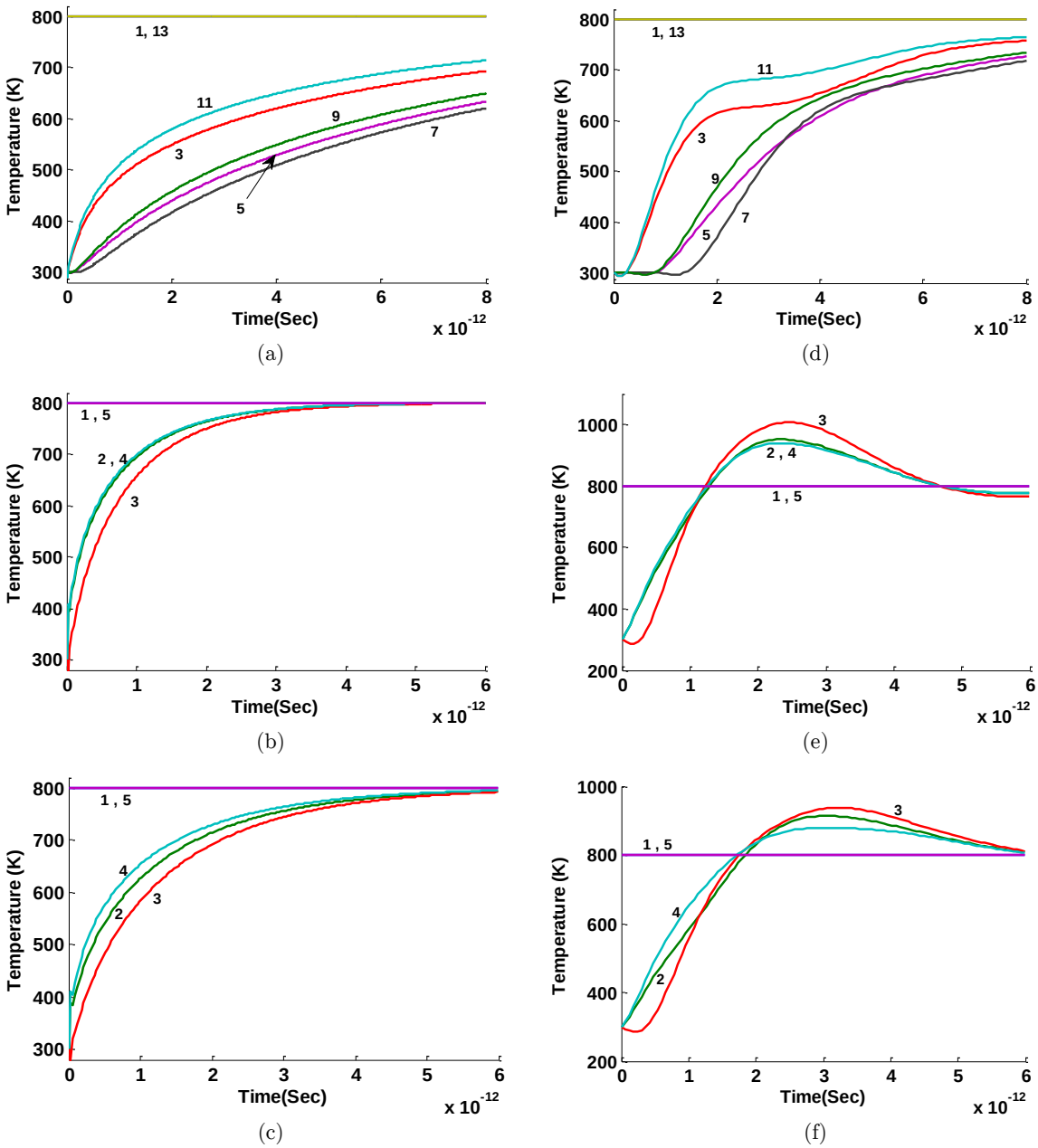

Figure 4: Fourier temperature distributions of examples (a) 1, (b) 2 and (c) 3 of MWCNTs under external and internal thermal shock. (d), (e) and (f) are, respectively, corresponding non-Fourier distributions.

With the non-Fourier heat conduction analysis, it is notable that the temperature of internal layers of examples 2 and 3 increases rapidly which reach to a higher temperature than the temperature of thermal shock source. This phenomenon can be explained only with wavelike behavior of heat transfer in the non-Fourier heat conduction analysis. Thus, thermal waves propagate from innermost and outermost layers toward internal layers. Thus, internal tubes are influenced by duplex thermal wave and as a result, their temperature increase intensely. Just similar to a spring

which is under initial displacement at both ends and binary displacement is occurred at the middle length of spring while the generated axial waves interference together. It is seen from Fig. 4 that maximum increase of internal layers temperature for examples 2 and 3 of MWCNTs are, respectively, about 40% and 30% greater than the temperature of thermal shock source. Therefore, it is concluded that in MWCNTs with the same thickness and under thermal shock on their innermost and outermost surfaces, greater temperature occurs in MWCNT with larger outermost diameter. But thermal waves in MWCNTs have damping behavior and become weak after passing from many layers. Therefore, as it is seen from Fig. 4, despite the non-Fourier heat conduction analysis, temperatures of internal tubes of 13-layer MWCNT do not increase as expected and the temperature of each layer is less than the temperature of thermal shock source. Thus, here, damping property of thermal waves overcomes the effect of their interference.

Generally, according to the non-Fourier heat conduction analysis, the internal temperatures of MWCNTs may be rise greater than the temperature of thermal shock source for a very few time. In order to explain this event, it is noted that according to Eq. (10) a relaxation time exist between temperature gradient and heat flow. Also, thickness of MWCNT may be so small that even this low delay time causes an intense increase of temperature. For better explanation of this concept, time histories of middle layer temperature and its gradient are compared in Fig. 5 for example 2 of MWCNTs under thermal shock on the internal and external surfaces. The illustrated temperature gradient in Fig. 5 is calculated by considering variations of temperature from the external surface to internal layers.

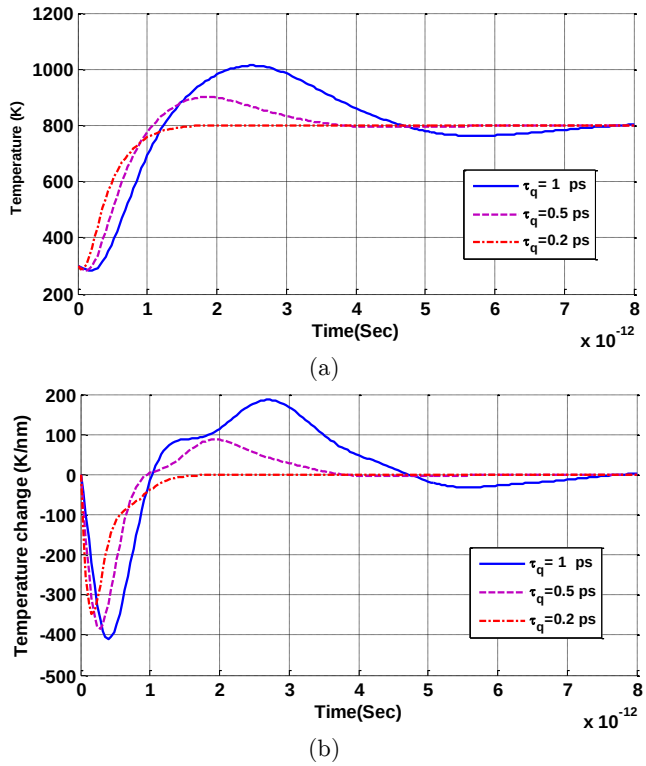

Figure 5: Time histories of middle layer (a) temperature and (b) its gradient, for example 2 of MWCNTs under thermal shock on the internal and external surfaces.

Thus, according to the Fourier heat conduction theory, when temperature gradient is negative, the temperature of internal tubes is lower than the temperature of outer tubes and heat flows towards the internal tubes and therefore, their temperatures must be increase. As soon as the sign of temperature gradient changes to positive, the temperature of internal tubes are greater than the temperature of outer tubes and thus, heat must flows from internal layers to outer layers and therefore, internal temperatures must be reduced. But as it is seen from Fig. 5, this process happens with a delay which is approximately equal to relaxation time τ_q. In fact, thickness of a MWCNT is so small that despite a tiny delay time, its inside temperature gradient is great enough for development intense temperature jump in initial instants and cause to increase temperature over than the temperature of thermal shock source. If these explanations are correct, with decreasing relaxation time, lower jump of temperature must be expected for internal layers. Fig. 5 confirms this idea and it is seen that by decreasing the relaxation time to 0.2 ps, the temperature of internal layers never reach the temperature of thermal shock source. Also by increasing dimensions, temperature gradient decreases and the same result must be observed. This case takes place in 13-layer MWCNT as it is seen from Fig. 4 that the temperature of none of layers reach the temperature of thermal shock source. For bodies with usual dimensions in meter-scale under thermal shock, generated temperature gradients are much smaller than those of CNTs. Hence, so extreme jumps of temperature do not happen.

3.2 Axial thermal shock

In this section, it is assumed that initial temperature of MWCNTs is 300 K and the temperature of one end of MWCNTs suddenly jumps to 800 K while the opposite end is kept at its initial temperature. Time histories of transient temperature at middle length of MWCNTs are shown in Fig. 6 which the effects of the Fourier and non-Fourier heat conduction analysis are compared for three mentioned examples of MWCNTs. For this case of thermal loading, because the thermal shock is applied to cross sectional area of all layers at the same time, heat flows along all layers simultaneously in axial direction and so, time histories of all layers approximately coincide to each other.

It is seen from Fig. 6 that by considering the Fourier heat conduction, temperature of middle length points start to rise as soon as thermal shock is applied. Moreover, the rate of temperature increment for examples 1 and 2 is lower than that of example 3. Therefore, it is revealed that the rate of temperature increment, decreases when the length of MWCNT increases. These behaviors can be explained only with the Fourier heat conduction analysis. According to this theory, heat flows with infinitive speed and so, from beginning of applying thermal shock, no point remains without any temperature changes. Since, longer MWCNT has more number of atoms; the longer MWCNT, the more time is needed for reaching the equilibrium state at any point.

Also, as illustrated in Fig. 6, with the non-Fourier heat conduction method, temperature of middle length points in MWCNTs start to increase with a time delay after applying the thermal shock. Furthermore, the rates of temperature increments are the same for all 3 examples. These behaviors are explanatory of heat wave propagation in axial direction of MWCNTs which can be explained only by the non-Fourier heat conduction analysis. As temperature variations of examples 1 and 2 are almost identical, it can be concluded that axial heat wave properties are approximately independent from radius and thickness of MWCNTs. Moreover, Fig. 6 shows that by

considering the non-Fourier heat conduction theory, temperature of examples 1 and 2 increase continuously until they reach to the equilibrium state. But in example 3, at initial moments, temperature rises immediately over 130% of the equilibrium temperature and then it decreases to its equilibrium value. Thus, in short length MWCNTs under one end thermal shock, temperature can become greater than the equilibrium temperature.

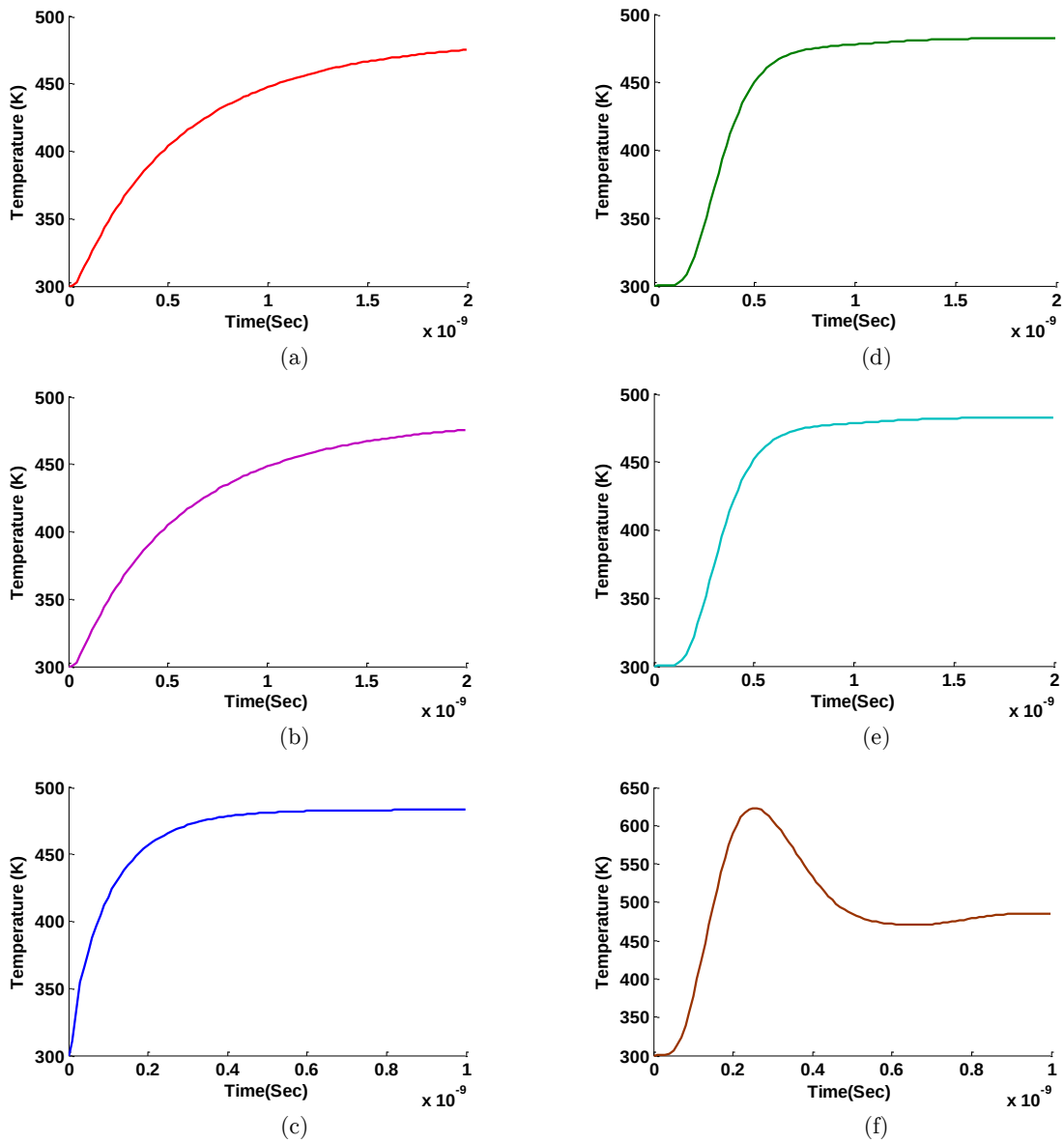

Figure 6: Fourier temperature distributions of examples (a) 1, (b) 2 and (c) 3 of MWCNTs under one end axially thermal shock. (d), (e) and (f) are, respectively, corresponding non-Fourier distributions.

In the next thermal loading case, it is assumed that MWCNTs are under both ends thermal shock synchronously. Temperature distributions in longitudinal directions are illustrated in Fig. 7

for three aforesaid examples of MWCNTs using the non-Fourier heat conduction analysis. These figures are plotted in four regular times with a time interval of Δt and are compared for states of one end and two ends thermal shock. The selected time interval values are 200ps, 400ps and 400ps , respectively, for examples 1 to 3 of MWCNTs under one end thermal shock and alternatively 150ps, 300ps and 300ps for both ends thermal shock.

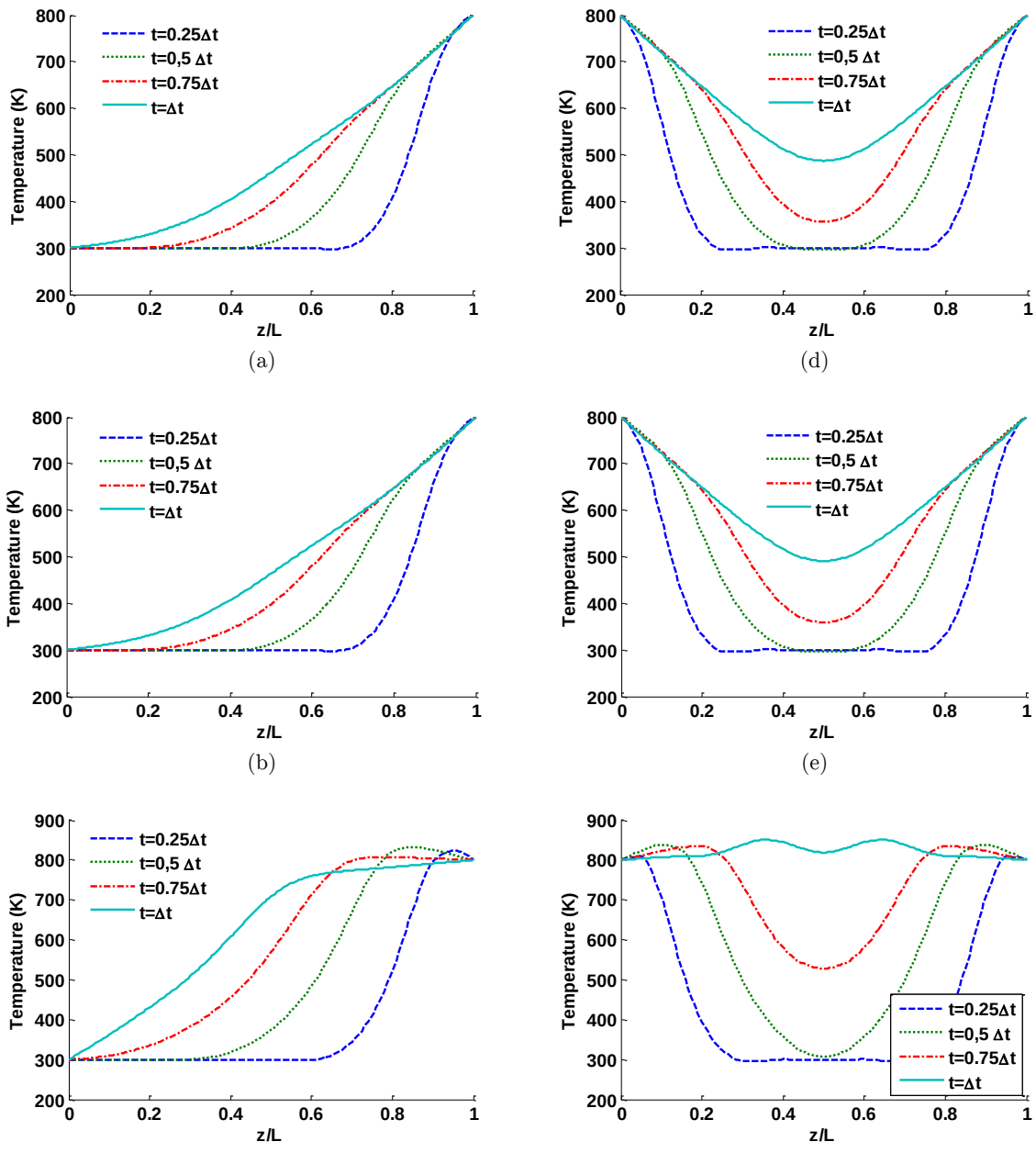

Figure 7: Temperature distributions thorough length of example (a) 1, (b) 2 and (c) 3 of MWCNTs under thermal shock on one end and (d), (e) and (f) are, respectively, corresponding distributions for thermal shock on two ends.

It is seen from Fig. 7 that when thermal shock is applied to both ends of MWCNTs, temperature increase of different points starts from shock source temperature and develop until all points reach to the equilibrium temperature. This behavior confirms thermal wave propagation in axial direction of MWCNTs according to the non-Fourier heat conduction theory. While thermal shock is applied to both ends of MWCNTs, the temperature of example 3 slightly increases higher than the temperature of thermal shock source. As length-to-diameter ratio in all three examples of MWCNTs are the same and the length of example 3 is lower than those of other examples, it can be concluded that because of occurring more intense temperature gradient in smaller CNTs, their internal temperature may be increase higher than the temperature of thermal shock source. As explained in previous section, it is due to the effects of relaxation time τ_q between temperature gradient and heat flow in nano-scale environments.

4 CONCLUSIONS

In the present work, the non-Fourier heat conduction equations are expanded and validated successfully for MWCNTs. A finite element model is developed to solve nonlinear equations and calculate transient temperature distribution in MWCNTs subjected to various thermal shock conditions. In this model, dependency of thermal properties on the size, direction and temperature is considered. The present results are compared with those obtained by the Fourier heat conduction analysis and it is concluded that with the Fourier heat conduction analysis, temperature of all points of a MWCNT is simultaneously affected from the thermal shock source. It is also found that as the size of a MWCNT increase, time rate of temperature increments decreases. However, for the non-Fourier heat conduction analysis, heat wave generates in location of thermal shock and propagates axially and radially. Therefore, time rate of temperature change of a point is approximately independent of MWCNT size.

Also, it is revealed that temperature gradients between sections of MWCNTs are size dependent and for small MWCNTs may be so much that cause to a significant temperature rise even higher than the temperature of thermal shock source. These situations are due to the effects of relaxation time between temperature gradient and heat flow, and generally are happened in synchronized thermal shocks applied on two different opposite surfaces of MWCNTs. Therefore, transient temperature distributions obtained by use of effective thermal properties and the Fourier heat conduction analysis, can be approximately accepted only for rather large and thick MWCNTs which are under thermal shock on one of their surfaces or cross sectional areas.

References

Aliev, A.E., Lima, M.H., Silverman, E.M., Baughman, R.H., (2010). Thermal conductivity of multi-walled carbon nanotube sheets: Radiation losses and quenching of phonon modes. Nanotechnology 21: 035709.

Ali Usmani, F., Hasan, M., (2010). Carbon nanotube field effect transistors for high performance analog applications: An optimum design approach. Microelectron. J 41: 395-402.

Bokobza, L., (2007). Multiwall carbon nanotube elastomeric composites: A review. Polymer 48: 4907-4920.

Cassell, A., Li, J., (2007). Carbon Nanotube Based Interconnect Technology: Opportunities and Challenges Micro- and Opto-Electronic Materials and Structures: Physics, Mechanics, Design, Reliability, Packaging, in: E. Suhir, Y.C. Lee, C.P. Wong (Eds.), Springer US, A181-A204.

Chang, C.W., Okawa, D., Garcia, H., Majumdar, A., Zettl, A., (2008). Breakdown of Fourier's Law in Nanotube Thermal Conductors. Phys. Rev. Lett. 101: 075903.

Dasgupta, K., Joshi, J.B., Banerjee, S., (2011). Fluidized bed synthesis of carbon nanotubes – A review, Chem. Eng. J. 171: 841-869.

Donadio, D., Galli, G., (2007). Thermal conductivity of isolated and interacting carbon nanotubes: Comparing results from molecular dynamics and the Boltzmann transport equation. Phys. Rev. Lett. 99.

Du, D., Wang, M., Zhang, J., Cai, J., Tu, H., Zhang, A., (2008). Application of multiwalled carbon nanotubes for solid-phase extraction of organophosphate pesticide. Electrochem. Commun. 10: 85-89.

Endo, M., Strano, M., Ajayan, P., (2008). Potential Applications of Carbon Nanotubes. Carbon Nanotubes. Springer Berlin / Heidelberg 13-61.

Fam, D.W.H., Palaniappan, A., Tok, A.I.Y., Liedberg, B., Moochhala, S.M., (2011). A review on technological aspects influencing commercialization of carbon nanotube sensors. Sens. Actuators, B 157: 1-7.

Fraysse, J., Minett, A.I., Jaschinski, O., Duesberg, G.S., Roth, S., (2002). Carbon nanotubes acting like actuators. Carbon 40: 1735-1739.

Giannopoulos, G.I., Kakavas, P.A., Anifantis, N.K., (2008). Evaluation of the effective mechanical properties of single walled carbon nanotubes using a spring based finite element approach. Comput. Mater. Sci. 41: 561-569.

González Noya, E., Srivastava, D., Chernozatonskii, L.A., Menon, M., (2004). Thermal conductivity of carbon nanotube peapods. Physical Review B 70: 115416.

Gu, Y., Chen, Y., (2007). Thermal conductivities of single-walled carbon nanotubes calculated from the complete phonon dispersion relations. Physical Review B - Condensed Matter and Materials Physics 76.

Guo, Z.X., Gong, X.G., (2009). Molecular dynamics studies on the thermal conductivity of single-walled carbon nanotubes. Frontiers of Physics in China 4: 389-392.

Hu, G.J., Cao, B.Y. (2012). Molecular dynamics simulations of heat conduction in multi-walled carbon nanotubes. Molecular Simulation 38: 823-829.

Jiang, W., Ding, G., Peng, H., (2009). Measurement and model on thermal conductivities of carbon nanotube nanorefrigerants. Int. J. Therm. Sci. 48: 1108-1115.

Jeng, Y.R., Tsai, P.C., Fang, T.H., (2004). Effects of temperature and vacancy defects on tensile deformation of single-walled carbon nanotubes. J. Phys. Chem. Solids 65: 1849-1856.

Kahaly, M.U., Waghmare, U.V., (2007). Size dependence of thermal properties of armchair carbon nanotubes: A first-principles study. Appl. Phys. Lett. 91.

Li, H., Sun, F.W., Liew, K.M., Liu, X.F., (2009). Stretching behavior of a carbon nanowire encapsulated in a carbon nanotube. Scr. Mater. 60: 129-132.

Lindsay, L., Broido, D.A., Mingo, N., (2010). Diameter dependence of carbon nanotube thermal conductivity and extension to the graphene limit. Physical Review B 82: 161402.

Lu, S., Cho, C., Choi, K.W., Choi, W., Lee, S., Wang, N., (2010). An inscribed surface model for the elastic properties of armchair carbon nanotube. J. Mech. Sci. Technol. 24: 2233-2239.

Maruyama, S., (2002). A molecular dynamics simulation of heat conduction in finite length SWNTs. Physica B 323: 193-195.

Moosaie, A., (2007). Non-Fourier heat conduction in a finite medium subjected to arbitrary periodic surface disturbance. Int. Commun. Heat Mass Transfer 34: 996-1002.

Nemilentsau, A.M., Slepyan, G.Y., Maksimenko, S.A., (2007). Thermal Radiation from Carbon Nanotubes in the Terahertz Range. Phys. Rev. Lett. 99: 147403.

Ni, X., Leek, M.L., Wang, J.S., Feng, Y.P., Li, B., (2011). Anomalous thermal transport in disordered harmonic chains and carbon nanotubes. Physical Review B 83: 045408.

Pettes, M.T., Shi, L., (2009). Thermal and structural characterizations of individual single-, double-, and multi-walled carbon nanotubes. Adv. Funct. Mater. 19: 3918-3925.

Ranjbartoreh, A., Wang, G., (2010). Consideration of mechanical properties of single-walled carbon nanotubes under various loading conditions. J. Nanopart. Res. 12: 537-543.

Reddy, J.N. (1993). An introduction to the finite element method. 2nd ed., McGraw-Hill, New York.

Savin, A.V., Hu, B., Kivshar, Y.S., (2009). Thermal conductivity of single-walled carbon nanotubes. Physical Review B - Condensed Matter and Materials Physics 80.

Shenogin, S., Xue, L., Ozisik, R., Keblinski, P., Cahill, D.G., (2004). Role of thermal boundary resistance on the heat flow in carbon-nanotube composites. J. Appl. Phys. 95: 8136-8144.

Shiomi, J., Maruyama, S., (2006). Non-Fourier heat conduction in a single-walled carbon nanotube: Classical molecular dynamics simulations. Physical Review B 73: 205420.

Talebian, S.T., Tahani, M., Abolbashari, M.H., Hosseini, S.M., (2012a). A glance on the effects of temperature on axisymmetric dynamic behavior of multiwall carbon nanotubes. Acta Mech. Sin. 28: 720-728.

Talebian, S.T., Tahani, M., Abolbashari, M.H., Hosseini, S.M., (2012b). An analytical solution for thermal shock analysis of multiwall carbon nanotubes. Comput. Mater. Sci. 61: 291-297.

Talebian, S.T., Tahani, M., Abolbashari, M.H., Hosseini, S.M., (2013). Response of multiwall carbon nanotubes to impact loading. Appl. Math. Model. 37: 5359-5370.

Talebian, S.T., Tahani, M., Hosseini, S.M., Abolbashari, M.H., (2010). Displacement time history analysis and radial wave propagation velocity in pressurized multiwall carbon nanotubes. Comput. Mater. Sci. 49: 283-292.

Thomas, J.A., Iutzi, R.M., McGaughey, A.J.H., (2010). Thermal conductivity and phonon transport in empty and water-filled carbon nanotubes. Physical Review B 81: 045413.

Volkov, A.N., Zhigilei, L.V., (2010). Scaling Laws and Mesoscopic Modeling of Thermal Conductivity in Carbon Nanotube Materials. Phys. Rev. Lett. 104: 215902.

Wang, B.L., Han, J.C., Sun, Y.G., (2012). A finite element/finite difference scheme for the non-classical heat conduction and associated thermal stresses. Finite Elem. Anal. Des. 50: 201-206.

Wang, C.C., (2010). Direct and inverse solutions with non-Fourier effect on the irregular shape. Int. J. Heat Mass Transfer 53: 2685-2693.

Wang, H.D., Cao, B.Y., Guo, Z.Y., (2010). Heat flow choking in carbon nanotubes. Int. J. Heat Mass Transfer 53: 1796-1800.

Wang, M., Guo, Z.Y., (2010). Understanding of temperature and size dependences of effective thermal conductivity of nanotubes. Phys. Lett. A 374: 4312-4315.

Wang, M., Yang, N., Guo, Z.Y., (2011). Non-Fourier heat conductions in nanomaterials. J. Appl. Phys. 110: 064310-064317.

Wang, Z., Devel, M., Dulmet, B., Stuart, S., (2009). Geometry-dependent nonlinear decrease of the effective young's modulus of single-walled carbon nanotubes submitted to large tensile loadings. Fullerenes Nanotubes and Carbon Nanostructures 17: 1-10.

Won, Y., Gao, Y., Panzer, M.A., Dogbe, S., Pan, L., Kenny, T.W., Goodson, K.E., (2012). Mechanical characterization of aligned multi-walled carbon nanotube films using microfabricated resonators. Carbon 50: 347-355.

Xu, M., Li, X., (2012). The modeling of nanoscale heat conduction by Boltzmann transport equation. Int. J. Heat Mass Transfer 55: 1905-1910.

Yang, D.J., Zhang, Q., Chen, G., Yoon, S.F., Ahn, J., Wang, S.G., Zhou, Q., Wang, Q., Li, J.Q., (2002). Thermal conductivity of multiwalled carbon nanotubes. Physical Review B - Condensed Matter and Materials Physics 66: 1654401-1654406.

Zhang, G., Li, B., (2005). Thermal conductivity of nanotubes revisited: Effects of chirality, isotope impurity, tube length, and temperature. J. Chem. Phys. 123: 1-4.

Zhang, X., Hu, M., Poulikakos, D., (2012). A Low-Frequency Wave Motion Mechanism Enables Efficient Energy Transport in Carbon Nanotubes at High Heat Fluxes. Nano Lett. 12: 3410-3416.

Zhu, S.Q., Wang, X., (2007). Effect of environmental temperatures on elastic properties of single-walled carbon nanotube. J. Therm. Stresses 30: 1195-1210.